The m^{6}A methyltransferase METTL3 modifies PGC-1α mRNA promoting mitochondrial dysfunction and oxLDL-induced inflammation in monocytes

Received for publication, March 16, 2021, and in revised form, July 8, 2021 Published, Papers in Press, August 8, 2021,
https://doi.org/10.1016/j.jbc.2021.101058

Xinning Zhang, Xin Li, Hongti Jia, Guoshun An, and Juhua Ni*

From the Department of Biochemistry and Biophysics, School of Basic Medical Sciences, Peking University, Beijing, China

Edited by Dennis Voelker

Mitochondrial biogenesis and energy metabolism are essential for regulating the inflammatory state of monocytes. This state is partially controlled by peroxisome proliferator-activated receptor gamma coactivator 1-alpha (PGC-1α), a coactivator that regulates mitochondrial biogenesis and energy metabolism. Disruption of these processes can also contribute to the initiation of chronic inflammatory diseases, such as pulmonary fibrosis, atherosclerosis, and rheumatoid arthritis. Methyltransferase-like 3 (METTL3)-dependent N^6-methyladenosine (m^{6}A) methylation has recently been shown to regulate a variety of inflammatory processes. However, the role of m^{6}A mRNA methylation in affecting mitochondrial metabolism in monocytes under inflammation is unclear, nor is there an established relationship between m^{6}A methylation and PGC-1α. In this study, we identified a novel mechanism by which METTL3 acts during oxidized low-density lipoprotein (oxLDL)-induced monocyte inflammation, where METTL3 and YTH N^6-methyladenosine RNA binding protein 2 (YTHDF2) cooperatively modify *PGC-1α* mRNA, mediating its degradation, decreasing PGC-1α protein levels, and thereby enhancing the inflammatory response. METTL3 coordinated with YTHDF2 to suppress the expression of *PGC-1α*, as well as that of cytochrome *c* (CYCS) and NADH:ubiquinone oxidoreductase subunit C2 (NDUFC2) and reduced ATP production and oxygen consumption rate (OCR). This subsequently increased the accumulation of cellular and mitochondrial reactive oxygen species (ROS) and the levels of proinflammatory cytokines in inflammatory monocytes. These data may provide new insights into the role of METTL3-dependent m^{6}A modification of *PGC-1α* mRNA in the monocyte inflammation response. These data also contribute to a more comprehensive understanding of the pathogenesis of monocyte-macrophage inflammation-associated diseases, such as pulmonary fibrosis, atherosclerosis, and rheumatoid arthritis.

Monocytes play an important role in the innate immune system and exhibit phagocytic activity to resist viral, bacterial, and fungal infections (1, 2). Circulating monocytes leave the bloodstream and migrate to inflamed tissues, where they can differentiate into macrophages or dendritic cells following stimulation by interaction with cytokines and/or microbial molecules (*e.g.*, complement proteins, bacterial flagellin, lipopolysaccharide) (2). Recruitment of monocytes is essential for effective control and clearance of pathogen infections, but persistent monocyte infiltration also contributes to the pathogenesis of chronic inflammatory and degenerative diseases, such as glomerulonephritis, pulmonary fibrosis, atherosclerosis, rheumatoid arthritis, and Alzheimer's disease (3–7). OxLDL is immunogenic and activates endothelial cells, monocytes/macrophages and T cells (8–10), but is toxic and can cause cell death at higher concentrations (8–10). Mitochondrial function and bioenergetics have gained recent attention for their contributions to chronic inflammatory diseases, as these processes—beyond their conventional role in generating energy—have been demonstrated to play critical roles in immunity (11, 12). For example, mitochondrial constituents (*e.g.*, mtDNA, mtROS, ATP, cardiolipin, N-formyl peptides) can activate innate immune receptors (*e.g.*, FPR1, NLRP3, NLRC4 and TLR9) to promote inflammatory responses. In addition, a change in mitochondrial metabolism can induce monocyte differentiation into different types of macrophages: M1 (proinflammatory) and M2 (anti-inflammatory) macrophages. M1 macrophages rely on glycolysis for energy production and, as such, have a lower ratio of oxidative phosphorylation to glycolysis. In contrast, M2 macrophages preferentially utilize oxidative phosphorylation and have a higher ratio of oxidative phosphorylation to glycolysis. PGC-1α (also known as PPARGC1A), a member of the peroxisome proliferator-activated receptor γ (PPARγ) coactivator family (13), transcriptionally regulates ~70% of respiratory chain complexes, as well as ATP synthases, tricarboxylic acid cycle intermediary enzymes, and fatty acid oxidation (14). Dysregulation of PGC-1α may induce aging, metabolic and degenerative diseases, as well as cancer in humans by suppressing mitochondrial biogenesis (15, 16). Interestingly, some studies have shown that PGC-1α may regulate inflammatory responses, such as its role in reprogramming energy metabolism of monocyte-macrophages during sepsis, beginning in the early stages of acute inflammation to later stages (17).

m^{6}A is one of the most prevalent posttranscriptional modifications in eukaryotic mRNA transcripts and impacts a

* For correspondence: Juhua Ni, juhuani@bjmu.edu.cn.

variety of physiological events (18). The level of m^{6}A methylation is dynamically mediated through the activity of methyltransferases (METTL3 and METTL14) and demethylases (FTO and ALKBH5) (19, 20). The m^{6}A modification functions by recruiting YT521-B homology (YTH) domain family proteins (*e.g.*, YTHDF1/2/3, YTHDC1/2) and IGF2BP family (IGF2BP1/2/3) proteins, as well as other factors (*e.g.*, eIF3) (20, 21). METTL3 is the core catalytic subunit of the m^{6}A methyltransferase complex, which plays a major catalytic role in m^{6}A modification. These m^{6}A-specific binding proteins either directly bind to m^{6}A or through indirect mechanisms to mediate RNA function or metabolism, including mRNA export, mRNA stability, mRNA splicing, mRNA translation, and mRNA decay (20, 21). Previous studies have demonstrated that m^{6}A modifications affect a diverse range of physiological and pathological processes, including spermatogenesis, neurogenesis, tumorigenesis, and immunoregulation (21–25). More recently, m^{6}A has been shown to play important roles in innate immunity. For example, METTL3 deficiency sustains long-chain fatty acid absorption by blocking the TRAF6-dependent inflammation response in lipopolysaccharide (LPS)-stimulated intestinal porcine epithelial cells (26). Another study has implicated METTL3-mediated alternative splicing of *MyD88* in the regulation of LPS-induced inflammatory response in human dental pulp cells. A shorter *MyD88* mRNA (MyD88S), lacking the second exon, exerts a dominant-negative effect on LPS-induced, TLR4-mediated signaling pathways and inhibits inflammatory cytokine production (27). Moreover, METTL3-mediated mRNA m^{6}A methylation promotes dendritic cell activation during LPS stimulation (28). These and other observations have suggested that the expression and functional role of METTL3 are complex and depend upon cell context, tissue type, individual developmental stage, and inflammation-stimulating factors. Although the role of METTL3 in inflammatory response in a variety of cells has been reported, the role of METTL3-mediated mRNA m^{6}A modification in mitochondrial function and metabolism during monocyte inflammation is unclear, especially, the functional linking between METTL3 and PGC-1α is not yet known.

In the present study, the association between METTL3 and mitochondrial metabolism in the context of monocyte inflammation was investigated. METTL3 associated with *PGC-1α* mRNA, thereby suppressing translation and protein expression. Moreover, knockdown of *METTL3* or *YTHDF2* increased both *PGC-1α* mRNA lifetime and expression, which reduced mitochondrial dysfunction and oxLDL-induced monocyte inflammation. These results suggest that the physical and functional interaction between METTL3 and PGC-1α is involved in monocyte inflammatory response. These data may contribute to a comprehensive understanding of the pathogenesis of monocyte-macrophage inflammation-associated diseases.

Result

METTL3 is upregulated in oxLDL-induced THP1 monocyte inflammation

To investigate the role of METTL3 in monocyte inflammation, THP-1 cells were treated with 20 μg/ml oxLDL and METTL3 was detected by immunoblot. Significantly higher levels of METTL3 were observed after oxLDL treatment for both 6 and 12 h (Fig. 1*A*). To confirm that oxLDL promotes inflammation, we measured mRNA levels of proinflammatory

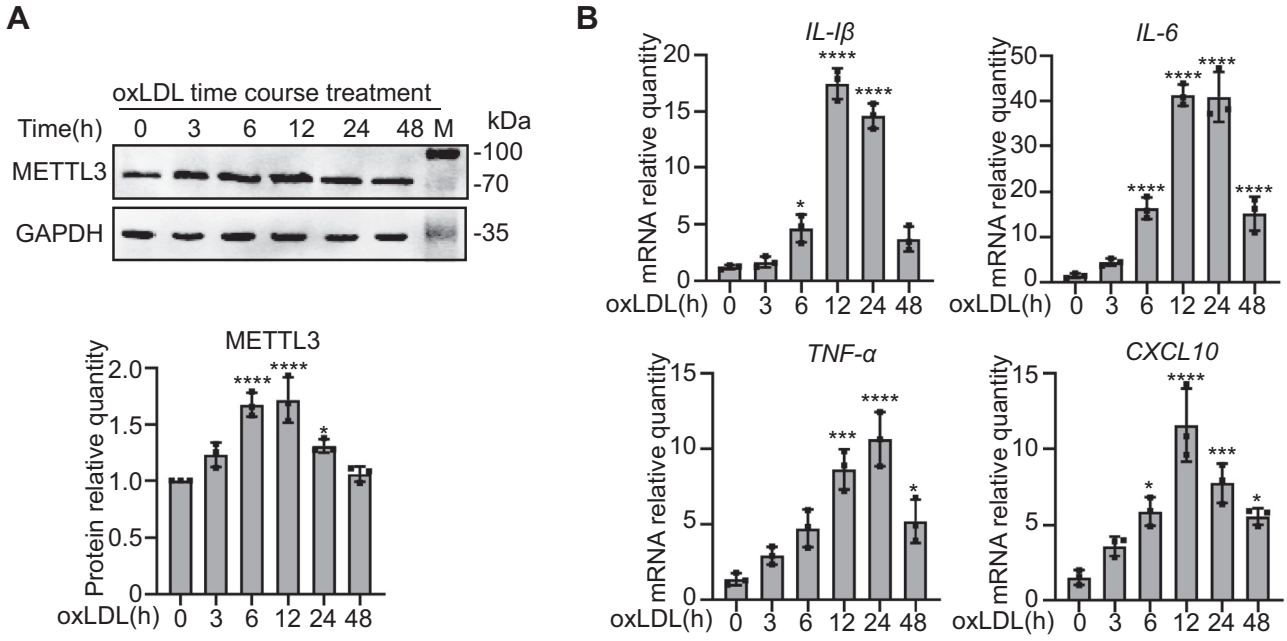

Figure 1. METTL3 is upregulated in oxLDL-induced THP1 monocyte inflammation. *A* and *B*, THP-1 cells were treated with 20 μg/ml oxLDL for 0, 3, 6, 12, 24, and 48 h. *A*, immunoblot detection of METTL3 protein levels of untreated and oxLDL-treated cells, with GAPDH as a loading control (n = 3). *B*, qRT-PCR determination of mRNA levels of *IL-1β*, *IL-6*, *TNF-α*, and *CXCL10* in response to oxLDL (n = 3). Data are represented as mean ± SD. *$p < 0.05$; **$p < 0.01$; ***$p < 0.001$; ****$p < 0.0001$ in all figures.

genes—including *IL-1β*, *IL-6*, *TNF-α*, and *CXCL10*—and found all four transcripts were significantly increased and reached a peak after being exposed to oxLDL for 12 and 24 h (Fig. 1*B*). METTL3 levels increased prior to oxLDL-induced inflammatory markers, suggesting a potential regulatory role in inflammation.

METTL3 inhibits the expression of energy metabolism genes

To probe downstream target genes of METTL3, the RNA-seq data set GES98623 (gene expression database GEO) was used to identify differentially expressed genes (DEGs) between control and silenced *METTL3* MOLM13 monocytes. From this analysis, 637 DEGs were identified, with 366 down-regulated and 271 upregulated genes. Interestingly, the expression of both *PGC-1α* and *PGC-1β* was upregulated (Fig. 2*A*). The CLIP-seq database POSTAR was used to identify 2121 genes that could be directly recognized and bound by METTL3, followed by pathway enrichment analysis using the online analysis tool DAVID that indicated correlation with the oxidative phosphorylation signaling pathway (Fig. 2*B*). Comparing the genes pulled from the POSTAR database to those correlated in pathway enrichment analysis and incorporating the DEGs from *METTL3*-silenced MOLM13 cells, we identified 11 candidate genes for interaction with *METTL3* that may be regulated by METTL3 (Table S1).

To explore the role of the 11 candidate genes, *METTL3* expression was silenced in THP-1 monocytes by *METTL3* siRNA. After silencing *METTL3* (Fig. S1*A*), the mRNA and protein levels of *PGC-1α*, *CYCS*, and *NDUFC2* were upregulated, whereas *COX7C*, *COX8A*, *NDUFA6*, *NDUFA12*, *NDUFAF1*, *NDUFB6*, *NDUFV3*, and *PGC-1β* were unchanged (Fig. 1, *C–E*). These data suggest that METTL3 may suppress the expression of *PGC-1α* and nuclear-encoded mitochondrial respiratory chain complex proteins *CYCS* and *NDUFC2*, thereby regulating energy metabolism.

METTL3 binds to the coding region of PGC-1α *mRNA and decreases its stability*

METTL3-dependent m^{6}A modification can influence mRNA stability, translation, and translocation (20, 21). As METTL3 ablation increased both mRNA and protein levels of PGC-1α, CYCS, and NDUFC2, we investigated the role of METTL3 in regulating PGC-1α, CYCS, and NDUFC2 expression at the posttranscriptional level. An anti-METTL3 antibody and primers specific to *PGC-1α*, *CYCS*, and *NDUFC2* were used in an RNA immunoprecipitation-qRT-PCR assay, revealing that *PGC-1α* mRNA, but not *CYCS* and *NDUFC2* mRNA, coprecipitated with METTL3 (Fig. 3*A*). Putative METTL3-binding sites on *PGC-1α* mRNA were identified using a sequence-based N^6-methyladenosine (m^{6}A) modification

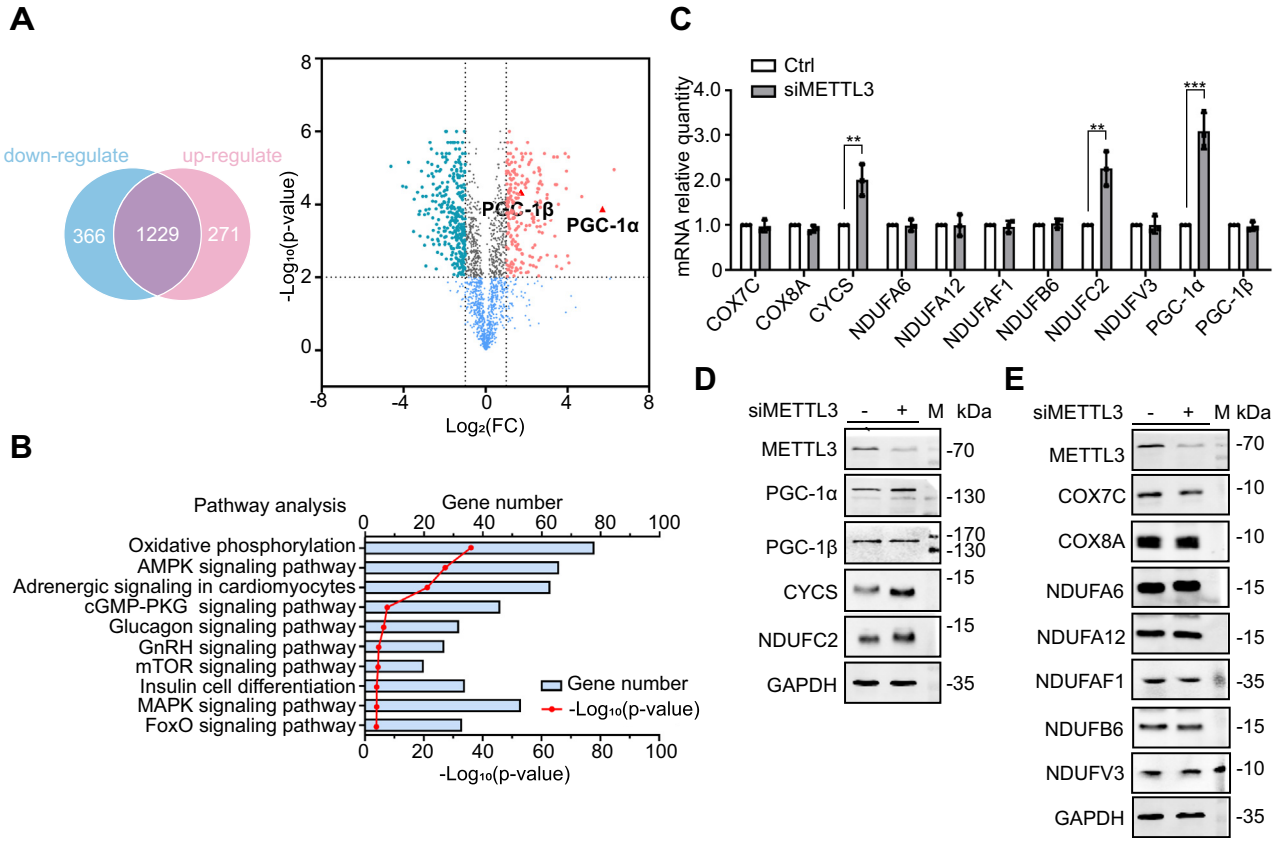

Figure 2. METTL3 inhibits the expression of energy metabolism genes. *A*, Venn diagram of upregulated and downregulated DEGs of siMETTL3 cells *versus* control cells. *B*, POSTAR online database pathway enrichment analysis. *C*, qRT-PCR determination of mRNA levels of various proinflammatory genes in *METTL3* knockdown cells (n = 3). *D* and *E*, immunoblot detection of various pro-inflammatory protein levels in control cells and *METTL3* knockdown cells (n = 3). Data are represented as mean ± SD. **p* < 0.05; ***p* < 0.01; ****p* < 0.001; ****p* < 0.0001 in all figures.

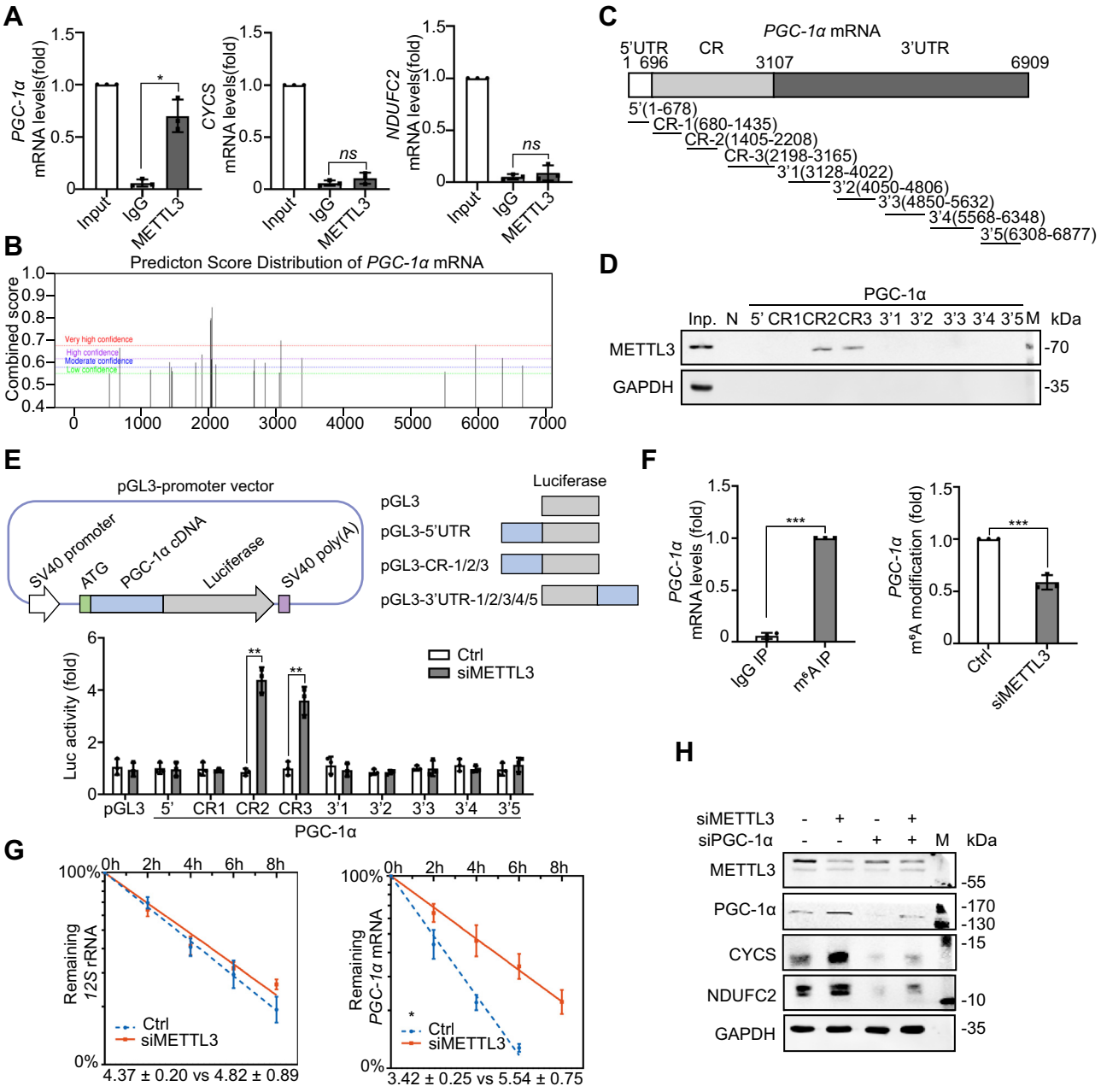

Figure 3. METTL3 binds to the coding region of *PGC-1α* mRNA and decreases its stability. *A*, RNA immunoprecipitation of various mRNAs with an anti-METTL3 antibody (n = 3). *B*, prediction sites of *PGC-1α* mRNA binding to METTL3 as produced from SRAMP. *C*, schematic of *PGC-1α* mRNA segments. *D*, RNA pull-down assays using THP-1 cell lysates and *in vitro*-transcribed RNA segments. Antisense sequence of *METTL3* served as the negative control [N], as well as a 5-μg aliquot input [Inp.] and GAPDH (n = 2). *E*, relative luciferase activities with *in vitro*-transcribed RNA segments in control and *METTL3* knockdown cells (n = 3). *F*, *PGC-1α* mRNA collected from a m^{6}A RNA immunoprecipitation assay with control and *METTL3* knockdown THP-1 cells using an IgG antibody or an anti-m^{6}A antibody (n = 3). *G*, degradation of *PGC-1α* mRNA and *12S* rRNA in control and *METTL3* knockdown cells, which was used to determine half-life (n = 3). *H*, immunoblot detection of various proteins in control, *METTL3* knockdown, *PGC-1α* knockdown, and *METTL3*/*PGC-1α* knockdown cells, with GAPDH as a loading control (n = 3). Data are represented as mean ± SD. *$p < 0.05$; **$p < 0.01$; ***$p < 0.001$; ****$p < 0.0001$.

site predictor (29). The predicted sites were mainly enriched in the coding sequence and 3′UTR of *PGC-1α* mRNA (Fig. 3*B*). These sequences were divided into nine segments—the 5′UTR, three segments of the coding region (CR), and five segments of the 3′UTR (Fig. 3*C*). RNA pull-down assays were performed using *in vitro*-transcribed, biotinylated fragments of these segments, revealing that METTL3 associated with the CR-2 and CR-3 fragments of *PGC-1α* mRNA (Fig. 3*D*). To test the functional association of METTL3 with the *PGC-1α* mRNA segments, pGL3-derived reporters bearing fragments of *PGC-1α* mRNAs were constructed to conduct an siRNA-repressible luciferase assay (Fig. 3*E*). 293T cells were transfected with the pGL3-PGC-1α constructs and a luciferase reporter construct. Luciferase activity increased after silencing *METTL3* in pGL3-derived reporters bearing *PGC-1α* CR-2 and CR-3 segments, but not with reporters containing segments that did not interact with METTL3 (Fig. 3*E*). This suggested that METTL3 expression was negatively associated with *PGC-1α* expression

and functioned through direct physical interaction in the coding region of *PGC-1α* mRNA. The role of METTL3-mediated m^{6}A modification in the regulation of *PGC-1α* mRNA was investigated using an m^{6}A-methylated RNA immunoprecipitation assay in order to analyze changes in m^{6}A modification in *PGC-1α* mRNA. In an *METTL3* knockdown model, there was a ~41% decrease in m^{6}A methylation for *PGC-1α* mRNA compared with the control group (Fig. 3*F*), indicating that *METTL3* knockdown reduced levels of *PGC-1α* mRNA m^{6}A modification.

As m^{6}A methylation regulates mRNA stability (21, 30), the enhanced *PGC-1α* mRNA expression in *METTL3*-silenced cells may have been due to increased stability of the unmethylated mRNA transcript. Silencing *METTL3* in THP-1 cells prolonged the half-life of *PGC-1α* mRNA from 3.4 h to 5.5 h, indicating that expression of METTL3 may reduce the stability of *PGC-1α* mRNA (Fig. 3*G*), which is consistent with upregulated *PGC-1α* mRNA and protein levels in *METTL3*-silenced cells. Although *PGC-1α* mRNA stability was linked to interaction with METTL3, the mechanism by which CYCS and NDUFC2 were upregulated after silencing *METTL3* is unknown. *PGC-1α* siRNA was used to silence *PGC-1α* expression in THP-1 cells (Fig. 3*H*), which decreased CYCS and NDUFC2 protein levels, indicating that the expression of *CYCS* and *NDUFC2* was dependent on the presence of PGC-1α and is indirectly affected by the presence of METTL3.

METTL3's regulation of PGC-1α is dependent on YTHDF2-based recognition of m^{6}A

YTHDF2 is an m^{6}A-binding protein that recognizes and destabilizes m^{6}A-modified mRNA (30). YTHDF2 recognition of *PGC-1α* mRNA was investigated by an RNA immunoprecipitation qRT-PCR assay, revealing that YTHDF2 can directly bind to *PGC-1α* mRNA (Fig. 4*A*). Similar to *METTL3* silencing, *YTHDF2* knockdown increased *PGC-1α* mRNA and protein levels (Fig. 4, *B* and *C*). RNA stability assays further demonstrated that *YTHDF2* knockdown increased the half-life of *PGC-1α* mRNA from 3.4 h to 6.1 h (Fig. 4, *D* and *E*). These results indicated that YTHDF2 may recognize the *PGC-1α* mRNA m^{6}A modification and induce degradation, a mechanism by which YTHDF2 and METTL3 may coordinately regulate *PGC-1α* mRNA stability and translation.

METTL3 and YTHDF2 promote oxLDL-induced mitochondrial dysfunction in monocytes

As PGC-1α has a role in mitochondrial biogenesis and energy metabolism, METTL3 and YTHDF2 might regulate ATP synthesis and ROS production of monocytes by targeting and destabilizing *PGC-1α* mRNA. THP-1 cell lines were generated by siRNA to knockdown *METTL3* alone, *METTL3/PGC-1α*, *YTHDF2* alone, and *YTHDF2/PGC-1α* and measured for ATP levels under treatment with a negative control or oxLDL.

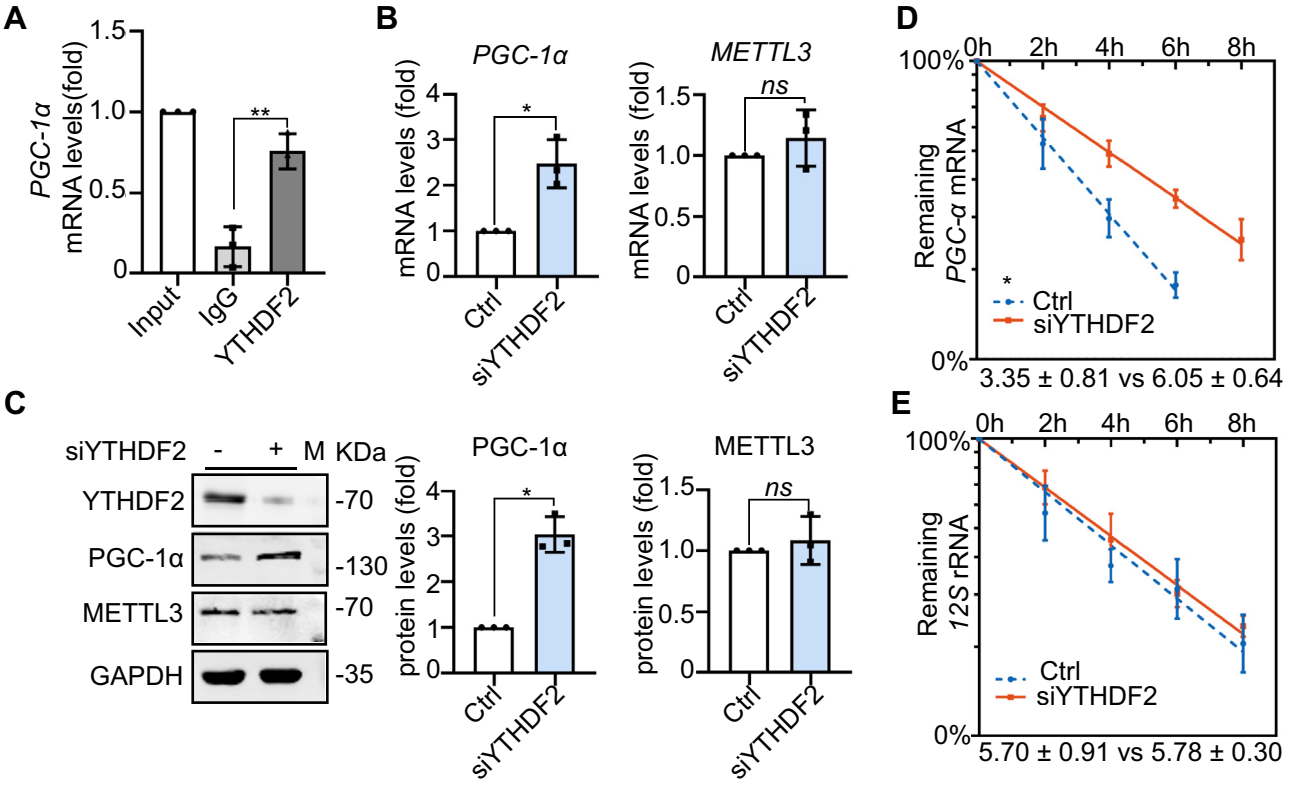

Figure 4. METTL3's regulation of PGC-1α is dependent on YTHDF2-based recognition of m^{6}A. *A*, *PGC1-α* mRNA collected from an RNA immunoprecipitation assay with THP-1 cells using an IgG antibody or an anti-YTHDF2 antibody (n = 3). *B*, qRT-PCR determination of mRNA levels of *PGC-1α* and *METTL3* in control and *YTHDF2* knockdown cells was detected by qRT-PCR (n = 3). *C*, immunoblot detection of various protein levels in control and *YTHDF2* knockdown cells lines, with GAPDH as a loading control (n = 3). *D* and *E*, half-lives of *PGC-1α* mRNA and *12S* rRNA in control and *YTHDF2* knockdown cells, which were used to determine half-life (n = 3). Data are represented as mean ± SD. *$p < 0.05$; **$p < 0.01$; ***$p < 0.001$; ****$p < 0.0001$.

METTL3 knockdown increased cellular ATP levels by 2-fold under both treatments, while knocking down both *PGC-1α* and *METTL3* attenuated this increase in ATP levels (Fig. 5*A*). Similar changes in ATP levels were observed in both the *YTHDF2* knockdown and knocking down both *YTHDF2* and *PGC-1α* (Fig. 5*C*). As increased levels of reactive oxygen species (ROS) are a marker of mitochondrial injury, flow cytometry was used to detect cellular and mitochondrial ROS levels. Interestingly, compared with untreated cells, cellular ROS levels in oxLDL-treated cells were increased by more than 2-fold, yet this increase was attenuated in *METTL3* or *YTHDF2* knockdowns when compared with oxLDL-treated cells transfected with scrambled (control) RNA. Meanwhile, knocking down *PGC-1α* at least partially abrogated the reduced cellular ROS levels in the *METTL3 or YTHDF2* knockdowns (Fig. 5, *B* and *D*). Similar changes in mitochondrial levels were observed in both knockdown *METTL3* alone, *METTL3/PGC-1α*, *YTHDF2* alone, and *YTHDF2/PGC-1α* (Fig. 5, *E* and *F*). To assess the role of METTL3 and YTHDF2 in mitochondrial function, we investigated oxygen consumption rate (OCR) in THP-1 cell knockdown of *METTL3* alone, *METTL3/PGC-1α*, *YTHDF2* alone, and *YTHDF2/PGC-1α*, which were detected by Seahorse extracellular flux analysis. As shown in Figure 5*G*, knockdown of *METTL3* or *YTHDF2* increased OCR and knockdown of *METTL3/PGC-1α* or *YTHDF2/PGC-1α* could reverse this effect. MitoTracker was also used to analyze mitochondria function in control cells, *METTL3* knockdown cells, and *YTHDF2* knockdown cells. As shown in Figure 5*H*, knocking down *METTL3* or *YTHDF2* caused increased fluorescence, indicating enhanced mitochondrial function, while the additional knockdown of *PGC-1α* impaired mitochondrial function. These results suggested that knocking down *METTL3* and *YTHDF2* promoted mitochondrial function by allowing *PGC-1α* translation.

METTL3 promotes oxLDL-induced inflammation of monocytes

METTL3 expression increased during oxLDL-induced monocyte inflammation (Fig. 1*A*). To investigate the role of METTL3 in monocyte inflammation, the mRNA and protein expression levels of proinflammatory cytokines *IL-1β*, *IL-6*, *TNF-α*, and *CXCL10* were measured in THP-1 cell knockdowns of *METTL3* and *METTL3/PGC-1α*. qRT-PCR assays revealed that *IL-1β*, *IL-6*, *TNF-α*, and *CXCL10* mRNA levels increased by 3.5–30-fold in control cells after 24 h of oxLDL treatment, while the *METTL3* knockdown decreased mRNA levels after oxLDL treatment, which was partially reversed in the *PGC-1α* double knockdown (Fig. 6*A*). Similar results were obtained *via* ELISA assay (Fig. 6*B*). These results indicated that METTL3 promoted, while PGC-1α suppressed, the inflammatory response induced by oxLDL treatment. In addition to proinflammatory cytokines, inflammatory monocytes express certain adhesion molecules under inflammation conditions (2, 5); therefore, we measured the expression of adhesion molecules *ICAM-1* and *MCP-1* by immunoblot. ICAM-1 and MCP-1 were markedly increased after oxLDL treatment, while knocking down *METTL3* significantly reduced the oxLDL-induced ICAM-1 and MCP-1 protein levels. This reduction was partially reversed in the *PGC-1α* double knockdown (Fig. 6*C*). In addition, monocyte-endothelial adhesion assays revealed decreased interaction between *METTL3* knockdown THP-1 cells and HUVEC cells, and this effect was reversed in the *PGC-1α* double knockdown (Fig. 6*D*). Taken together, these results indicated that METTL3 promoted oxLDL-induced mitochondrial dysfunction and inflammation of monocytes.

Discussion

In addition to mediating host antimicrobial defense, monocytes also contribute to many inflammatory diseases (3–7, 31). Recently, METTL3 was shown to be involved in inflammatory responses in preosteoblasts (32), dental pulp cells (27), and epithelial cells (26), although little is known about the role of METTL3 in monocyte inflammation. In this study, we demonstrate that inflammatory stimulator-induced METTL3 promotes mitochondrial dysfunction and inflammatory response in monocytes *via* suppressing *PGC-1α*. We have identified a new mechanism underlying METTL3 acting in monocyte inflammation, in which METTL3 interacts with *PGC-1α* mRNA to mediate its m^{6}A modification. YTHDF2 selectively recognizes m^{6}A modification to mediate *PGC-1α* mRNA degradation. Subsequently, suppression of *PGC-1α* by METTL3 leads to inhibiting the expression of nuclear-encoded mitochondrial respiratory chain protein-related genes *CYCS* and *NDUFC2*, thereby reducing ATP production and increasing ROS accumulation in inflammatory monocytes (Fig. 7). These data may provide new insight into the role of METTL3-dependent m^{6}A modification of *PGC-1α* mRNA in monocyte inflammatory response and aid in better understanding of pathogenesis of monocyte-macrophage inflammation-related diseases.

The functional outcomes of m^{6}A modification are extensive and determined by the dynamic balance of m^{6}A RNA-specific binding proteins (m^{6}A readers) and the type of modified RNAs (20, 30). The most common m^{6}A readers, YTHDF1, YTHDF2, and YTHDF3, are mainly distributed in the cytoplasm and have different functions. YTHDF1 enhances translation by interacting with translation initiating factors and ribosomes. YTHDF3 interacts with both YTHDF1 and YTHDF2 to assist with regulation of mRNA fate. YTHDF2 specifically recognizes mRNA m^{6}A sites in the stop codon region, the 3′UTR, and the coding region to promote target m^{6}A RNA degradation (30). The C-terminal domain of YTHDF2 selectively binds to m^{6}A RNAs, while the N-terminus brings the YTHDF2-mRNA complex to RNA decay sites in the cytosol and recruits the CCR4-NOT deadenylase complex to the RNA (33). As observed with other mRNA transcripts, YTHDF2 targeted m^{6}A methylation and mediated *PGC-1α* mRNA degradation, thereby decreasing *PGC-1α* mRNA lifetime and protein expression. In contrast, knocking down either *METTL3* or *YTHDF2* increased mRNA lifetime and protein levels. Study data indicated that the METTL3 regulatory effects on *PGC-1α* expression depended upon the m^{6}A reading function of

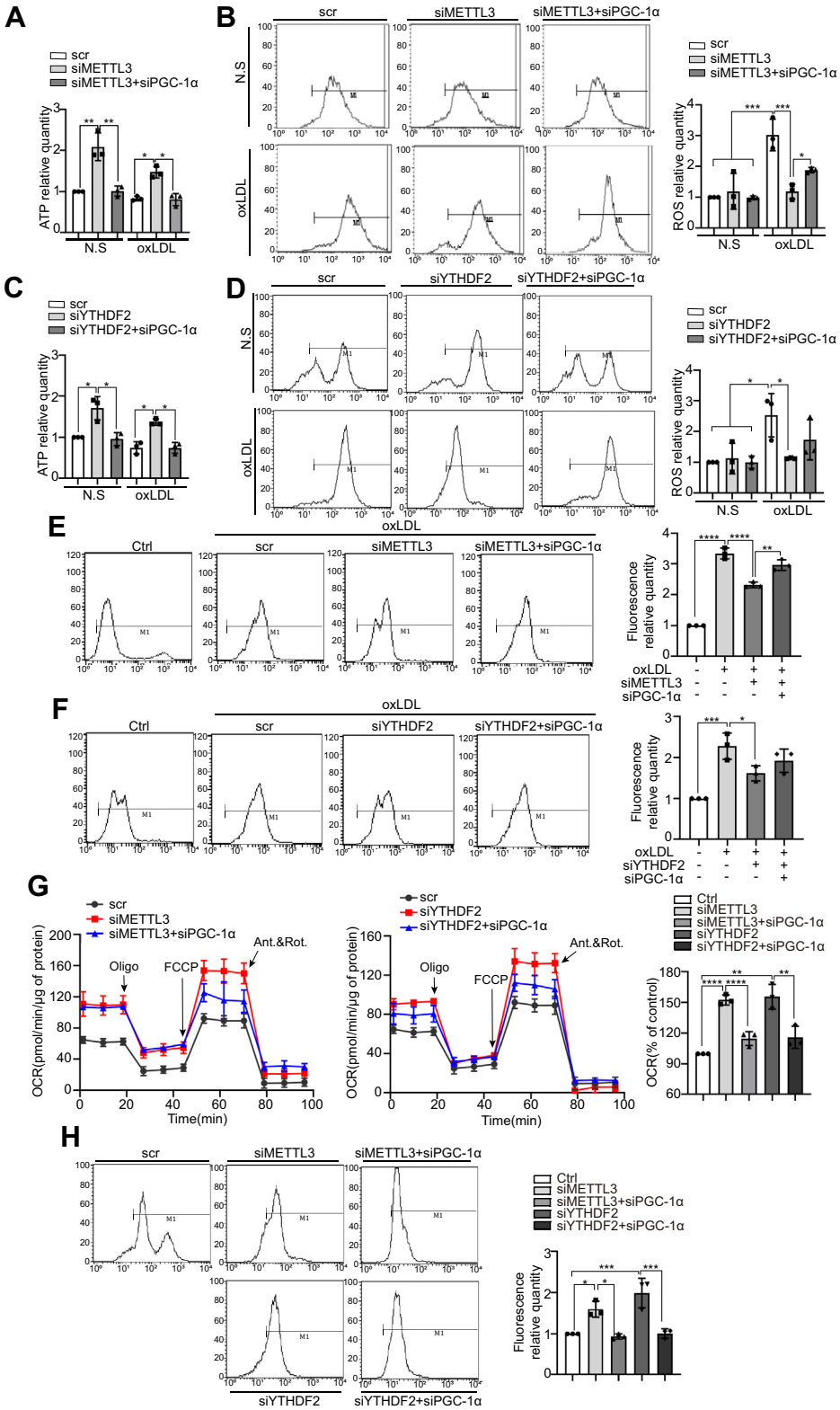

Figure 5. METTL3 and YTHDF2 promote oxLDL-induced mitochondrial dysfunction in monocytes. *A*, intracellular ATP levels in control, *METTL3* knockdown, and *METTL3*/*PGC-1α* knockdown cells both untreated and treated with oxLDL (n = 3). *B*, cellular ROS levels in control, *METTL3* knockdown, and *METTL3*/*PGC-1α* knockdown cells both untreated and treated with oxLDL (n = 3). *C*, intracellular ATP levels in control, *YTHDF2* knockdown, and *YTHDF2*/*PGC-1α* knockdown cells both untreated and treated with oxLDL (n = 3). *D*, cellular ROS levels in control, *YTHDF2* knockdown, and *YTHDF2*/*PGC-1α* cells both untreated and treated with oxLDL (n = 3). *E*, mitochondrial ROS levels in control untreated with oxLDL, control, METTL3 knockdown, and METTL3/PGC-1α knockdown cells treated with oxLDL (n = 3). *F*, mitochondrial ROS levels in control untreated with oxLDL, control, YTHDF2 knockdown, and YTHDF2/PGC-1α cells treated with oxLDL (n = 3). *G*, OCR in control, METTL3 knockdown, and METTL3/PGC-1α cells (n = 3) and OCR in control, YTHDF2 knockdown, and YTHDF2/PGC-1α knockdown cells (n = 3). *H*, THP-1 cells were transfected with scrambled RNA, *METTL3* siRNA, *YTHDF2* siRNA, and *PGC-1α* siRNA for 48 h and then were labeled with MitoTracker fluorescence intensity in control, *METTL3* knockdown, *METTL3*/*PGC-1α*, *YTHDF2* knockdown, and *YTHDF2*/*PGC-1α* knockdown cell (n = 3). Data are represented as mean ± SD. *$p < 0.05$; **$p < 0.01$; ***$p < 0.001$; ****$p < 0.0001$.

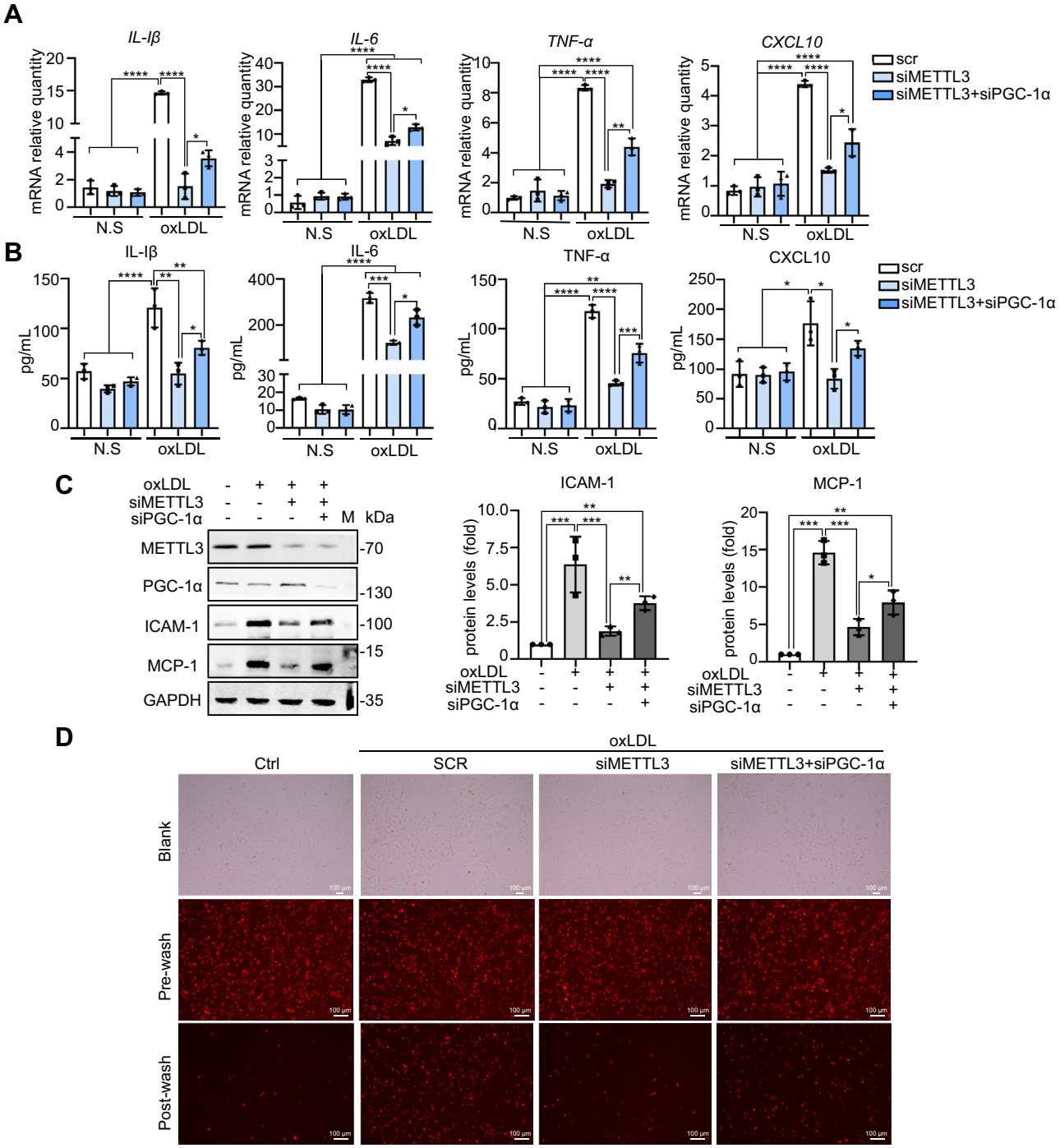

Figure 6. METTL3 promotes oxLDL-induced inflammation of monocytes. *A*, qRT-PCR determination of mRNA levels of *IL-1β*, *IL-6*, *TNF-α*, and *CXCL10* in *METTL3* knockdown and *METTL3/PGC-1α* knockdown cells both untreated and treated with oxLDL (n = 3). *B*, ELISA detection of protein levels of IL-1β, IL-6, TNF-α, and CXCL10 in control, *METTL3* knockdown, and *METTL3/PGC-1α* knockdown cells both untreated and treated with oxLDL (n = 3). *C*, immunoblot detection of various protein levels in control, *METTL3* knockdown, and *METTL3/PGC-1α* knockdown cells both untreated and treated with oxLDL (n = 3). *D*, monocyte-endothelial adhesion assay and fluorescence of untreated control cells and control *METTL3* knockdown, and *METTL3/PGC-1α* knockdown cells treated with oxLDL (n = 3, scale bar: 100 μm). Data are represented as mean ± SD. *$p < 0.05$; **$p < 0.01$; ***$p < 0.001$; ****$p < 0.0001$.

YTHDF2. YTHDF3 may also play a role in this process. Knocking down the demethylase *FTO* increases the m^{6}A methylation level of *PGC-1α* mRNA and decreases the expression of *PGC-1α* (34). As such, other factors may participate in METTL3-mediated *PGC-1α* mRNA degradation.

PGC-1α regulates gene networks involved in mitochondrial biogenesis and energy metabolism by interacting with a number of coactivator complexes containing chromatin remodeling activities (*e.g.*, CBP/p300 and GCN5), transcription factor families (NRF-1, PPARα, YY1, and MEF2C), and nuclear hormone receptor families (ERRs) (35). Dysregulation of *PGC-1α* may lead to mitochondrial dysfunction and disturb mitochondrial oxidative phosphorylation, TCA cycle reactions, and fatty acid oxidation (14, 35). In this study, METTL3

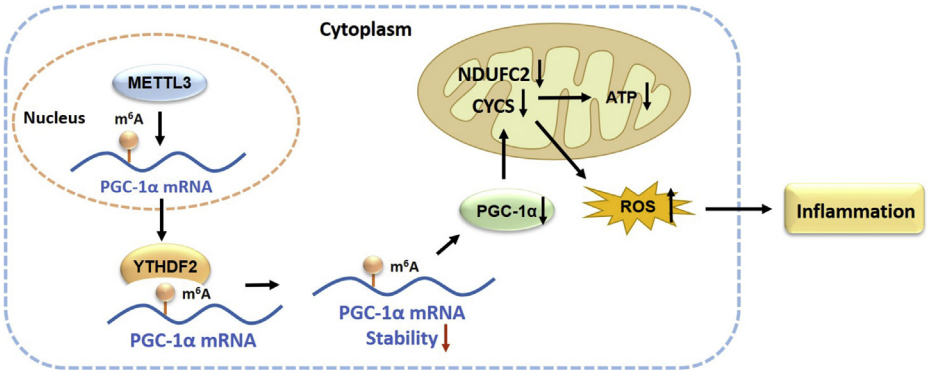

Figure 7. A working model depicting the role and the mechanism of METTL3 in promoting mitochondrial dysfunction and monocyte inflammation by *PGC-1α* suppression. METTL3 acts in monocyte inflammation, in which METTL3 interacts with *PGC-1α* mRNA to mediate m^{6}A modification; YTHDF2 selectively recognizes m^{6}A modification to mediate *PGC-1α* mRNA degradation, by which YTHDF2 and METTL3 coordinately reduce the lifetime of *PGC-1α* mRNA. Subsequently, suppression of *PGC-1α* by METTL3 leads to inhibition of the expression of nuclear-encoded mitochondrial respiratory chain protein-related genes *CYCS* and *NDUFC2*, thereby reducing ATP production and increasing ROS accumulation in inflammatory monocytes.

methylation was determined to be necessary for YTHDF2 suppression of the expression of *PGC-1α*, *CYCS*, and *NDUFC2*, which was related to mitochondrial dysfunction in oxLDL-stimulated monocytes. The mitochondrial dysfunction may be due to PGC-1α-induced downregulation of *CYCS* and *NDUFC2* genes in monocytes during oxLDL-induced acute inflammation. CYCS is a central component of the electron transport chain, *i.e.*, the ubiquinol cytochrome *c* reductase (mitochondrial complex III), transferring electrons from cytochrome *b* (one subunit of complex III) to the cytochrome oxidase complex (complex IV). The nuclear respiratory factor 1 (NRF-1) bound to the upstream region of the *CYCS* promoter is required for *CYCS* gene activation (36). PGC-1α can directly interact with NRF-1 to activate the *CYCS* gene (35). NDUFC2 is one of the subunits of mitochondrial complex I, and the CCAAT/enhancer-binding protein alpha (C/EBPα) can trigger aberrant expression of NADH dehydrogenase-encoding genes, including *NDUFC2* and *NDUFA1* (37). The prediction of the transcription factor binding sites by QIAGEN in the *NDUFC2* gene promoter shows potential binding motifs for PPARγ, c-Myc, HFH-1, HOXA3, Max, NF-1, and Pax-5. PGC-1α has been identified as a coactivator of PPARγ (38) and increases *PPARα* transcriptional activity, as well as promotes interactions with a variety of transcription factors and proteins (39). Therefore, it is reasonable to infer that NDUFC2 could be a potential target of PGC-1α, although the relationship between the two molecules is not clear. Taken together, these findings suggest that CYCS and NDUFC2 were downregulated in oxLDL-induced inflammatory monocytes when *PGC-1α* was suppressed by METTL3 with YTHDF2. Reduction of *PGC-1α*, *CYCS*, and *NDUFC2* impairs electron transport and oxidative phosphorylation (a major source for ATP production), thereby reducing mitochondrial ATP synthesis and increasing ROS production, ultimately causing inflammation (40).

In summary, we demonstrated that METTL3 promoted mitochondrial dysfunction and inflammatory response during oxLDL-induced inflammation in monocytes. METTL3 caused m^{6}A methylation of *PGC-1α* mRNA, as knockdown of *METTL3* suppressed oxLDL-induced monocyte inflammation and protected mitochondrial function against oxLDL-induced inflammation. These data may provide new insights into the role of METTL3-dependent m^{6}A modification of *PGC-1α* mRNA in monocyte inflammation and provide additional information into the pathogenesis of monocyte-macrophage inflammation-related diseases

Experimental procedures

Cell culture and treatment

THP-1 cells were cultured in RPMI-1640 (Roswell Park Memorial Institute) media (Invitrogen) with 1.5 g $NaHCO_3$/L and supplemented with 10% fetal bovine serum (FBS) at 37 °C in 5% CO_2, with 100 U/ml penicillin and 100 μg/ml streptomycin. 293T cells were cultured in Dulbecco's modified Eagle's medium (Invitrogen) with 1.5 g $NaHCO_3$/L and supplemented with 10% FBS at 37 °C in 5% CO_2, with 100 U/ml penicillin and 100 μg/ml streptomycin. Human umbilical vein endothelial cells (HUVECs) were isolated from segments of human umbilical cord vein by collagenase digestion and cultured in medium 199 (Gibco) supplemented with 10% FBS. Cells between passages 2 and 4 were used for the experiments.

For plasmid transfections, Lipofectamine 2000 (Invitrogen) was used following the manufacturer's instructions. Cells were harvested 48 h after transfection for further analysis. *METTL3* (1# 5′-AGGAGCCAGCCAAGAAAUCAATT-3′, 2# 5′-GCAC TTGGATCTACGGAAT-3′) siRNA, *PGC-1α* (1# 5′-CCAAGA CUCUAGACAACUATT-3′, 2# 5′-UUUCUGGGUGGAUU-GAAGUGGUGUA-3′) siRNA, *YTHDF2* (1# 5′-CAAGGAAA CAAAGTGCAAA-3′, 2# 5′- AAGGACGTTCCCAATAGCC AA-3′) siRNA or a control siRNA (AAGAGGCAAUUAC-CAGUUUCA) was transfected using RNAimax (Invitrogen) following the manufacturer's instructions. Cells were harvested 72 h after transfection for further analysis.

For preparing monocyte inflammation model, THP-1 cells were treated with 20 μg/ml oxLDL (Meilunbio) for given hour(s) and harvested for the next experiments.

Data resources and bioinformatics analysis

RNA-seq of human myeloid leukemia cells was obtained from data set GSE98623 in the GEO Database (https://www.

ncbi.nlm.nih.gov/geo/). CLIP-seq of METTL3 was from the database POSTAR (http://lulab.life.tsinghua.edu.cn/postar/), and pathway enrichment analysis was conducted using the online analysis tool DAVID (https://david.ncifcrf.gov/).

Western blot analysis

Western blot analysis was performed using standard procedures (41). Briefly, the collected cells were washed three times with cold PBS on ice and placed in 3-fold cold lysis buffer. The suspension was vortexed. The lysate was centrifugated at 4 °C, 12,000 rpm for 20 min in an Eppendorf microcentrifuge, and the supernatant was collected for measurement of protein concentration by BCA Protein Assay Kit (Thermo Fisher Scientific-CN). Then after, 6× protein loading buffer was added and incubated in 98 °C water for 10 min. Thirty micrograms of proteins were subjected to 10% SDS-PAGE and transferred onto nitrocellulose membranes, blocked with 5% nonfat milk in TBS-T (20 mM Tris, 500 mM NaCl, and 0.1% Tween 20) at room temperature for 2 h with rocking. The membranes were probed with specific antibodies overnight at 4 °C. After washing with 5% nonfat milk/TBS-T three times for 15 min each, membranes were incubated with fluorescently labeled secondary antibodies (LICOR, USA) in 5% nonfat milk/TBS-T at room temperature for 1 h. After washing with TBS-T, the protein–antibody complex was detected by Odyssey two-color infrared laser imaging system (LICOR, USA).

Monoclonal anti-METTL3, monoclonal anti-GAPDH, and monoclonal anti-YTHDF2 were bought from Abcam. Monoclonal anti-PGC-1β, monoclonal anti-CYCS, monoclonal anti-MCP-1, monoclonal anti-NDUFC2, and monoclonal anti-NDUFB6 were bought from Santa Cruz. Monoclonal anti-COX8A, monoclonal anti-NDUFA6, monoclonal anti-NDUFA12, and monoclonal anti-ICAM-1 antibodies were bought from Abclonal. Monoclonal anti-PGC-1α antibodies were from Merck Millipore.

RNA isolation, reverse transcription, and quantitative real-time qPCR analysis

Total cellular RNA was extracted using TRIzol (Invitrogen) and treated with reverse transcriptase and a mixture of oligo-dT and random hexamers (Invitrogen). To quantify the levels of different mRNAs, qRT-PCR analysis was performed using the primer pairs (Table S2) listed in the supporting information.

Preparation of transcripts

cDNA was used as a template for PCR amplification of RNA fragments. All primers contained the T7 promoter sequence (5′-CCAAGCTTCTAATACGACTCACTATAGGGAGA-3′). The *in vitro* transcription reaction (1 μl 10 mmol/L ATP, 1 μl 10 mmol/L GTP, 1 μl 10 mmol/L CTP, 0.5 μl 10 mmol/L UTP, 0.5 μl 10 mmol/L Biotin-11-UTP, 1 μg DNA templet, 4 μl 5× buffer, 1 μl T7 RNA polymerase, 2 μ1 100 mmol/L DTT, 1 μl RNA inhibitor, added DEPC H_2O to 50 μl) was performed in a 37 °C water bath for 6–8 h. and then, biotin-labeled RNA probes were purified and the concentration of probes were determined.

Constructs and luciferase reporter assay

To construct pGL3-derived reporter vectors, the fragments of *PGC-1α* mRNA 5′UTR were inserted between the HindIII and NcoI sites of a pGL3-promoter vector (Promega). The CR and 3′UTR fragments were inserted into the FseI and XbaI sites of a pGL3-promoter vector (Promega). 293T cells were seeded in 24-well plates (4×10^4 cells per well). Cells were transfected with siRNA targeting *METTL3*. After 24 h, cells were transfected with each of the pGL3-derived reporters and cultured for an additional 48 h. Firefly and renilla luciferase activities were measured with a double luciferase assay system (Promega) following the manufacturer's instructions. All firefly luciferase measurements were normalized to renilla luciferase measurements from the same sample.

RNA pull-down assays

PCR-amplified DNA fragments were used as templates to transcribe biotinylated RNA by using T7 RNA polymerase in the presence of biotin-UTP. One microgram of purified biotinylated transcripts was incubated with 30 mg of cell lysates for 30 min at room temperature. Complexes were isolated with paramagnetic streptavidin-conjugated Dynabeads (Dynal), and the pull-down material was analyzed by western blot.

RNA immunoprecipitation

A total of 5×10^7 THP-1 cells were collected and lysed in a buffer containing 150 mmol/L KCl, 10 mmol/L HEPES (pH 7.6), 2 mmol/L EDTA, 0.5% CA-630, 0.5 mmol/L DTT, 1:100 protease inhibitor cocktail, and 400 U/ml RNase inhibitor. The cell lysate was incubated with METTL3 beads at 4 °C for 4 h, followed by washing the beads with NT2 buffer, and incubation in elution solution. After washing, bound RNAs were extracted using TRIzol reagent and analyzed by qRT-PCR.

m^6A-IP

Total RNA was extracted from THP-1 cells with TRIzol (Invitrogen), and additional DNase I was applied to all samples to avoid DNA contamination. Enrichment of m^6A-containing transcript segments was analyzed through qRT-PCR.

RNA half-life analysis

To determine the half-life of *PGC-1α* mRNAs, actinomycin D (final concentration 2 μg/ml, Amresco) was added to THP-1 cell cultures. Following 48 h of siRNA transfection, the total RNAs were extracted at 0, 2, 4, 6, and 8 h after actinomycin D treatment. The mRNA levels at different times were analyzed by qRT-PCR.

Cytokine ELISA assays

Cells were incubated in RPMI1640 with 10% FBS and were treated with 20 μg/ml oxLDL for 24 h. Postculture media was

then collected and subjected to ELISA assays specific for IL-1β, IL-6, TNF-α, and CXCL10 (Abclonal).

ATP level determination

For measuring ATP levels, an ATP Bioluminescent Assay Kit (Sigma) was used following the manufacturer's instructions.

Measurement of cellular ROS

For live cell analysis, THP-1 cells were cultured in a 6-well plate at a density of 2×10^5 cells/well and incubated in RPMI1640/10% FBS in the presence of 10 μmol/L carboxy-DCFDA (Beyotime) for 20 min at 37 °C to assess total cellular ROS. At the end of incubation, cells were collected and suspended in 200 μl buffer and immediately subjected to flow cytometry analysis. Carboxy-DCFDA fluorescence was detected with the FITC channel.

Measurement of mitochondrial ROS

For live cell analysis, THP-1 cells were cultured in a 6-well plate at a density of 2×10^5 cells/well and were transfected with siRNA for 48 h. Before the experiment, the cells were stained with 5 μM MitoSox Red (yeasen) for mitochondria. They were then treated per the manufacturer's protocol in the cellular retention assay. Data were collected using flow cytometry analysis. The fluorescence of MitoTracker Red (red) was excited at 510 nm and measured at 580 nm.

MitoTracker staining

For live cell analysis, THP-1 cells were cultured in a 6-well plate at a density of 2×10^5 cells/well and were transfected with siRNA for 48 h. Before the experiment, the cells were stained with 50 nM MitoTracker Red (Solarbio) for mitochondria and then were treated per the manufacturer's protocol in the cellular retention assay. Data were collected by using flow cytometry analysis. The fluorescence of MitoTracker Red (red) was excited at 579 nm and collected at 599 nm.

Monocytes energetics

THP-1 cells were seeded into the specialized XFe24 cell culture microplate (Seahorse Bioscience) at about 50,000–80,000 cells/well. THP-1 cells were transfected with METTL3 and PGC-1α siRNA for 24 h and treated with 20 μg/ml oxLDL for 24 h. The OCR was measured using a Seahorse Bioscience Extracellular Flux Analyzer (Agilent) and Seahorse XF Cell Mito Stress Test Kit (Agilent). Cells were then lysed in RIPA buffer and subjected to Bradford protein assay (Bio-Rad). OCR values were normalized by protein values in each well.

Adhesion assay

In total, 3×10^4 HUVECs were plated per well in a 24-well plate (Corning) in M199 and grown to complete confluence. THP-1 cells were transfected with *METTL3* and *PGC-1α* siRNA for 24 h and were treated with 20 μg/ml oxLDL for 24 h. THP-1 monocytes were labeled with 5 mmol/L of CellTracker CM-DiI (Invitrogen) in parallel according to the manufacturer's instructions. A total of 0.5×10^6 labeled THP-1 monocytes were added per well in a 24-well plate and incubated for 30 min in 5% CO_2 at 37 °C. After incubation, each well was washed three times with 500 μl M199, and ten high-power field digital images were taken using an inverted fluorescence microscope (Lecia).

Statistics

All data are presented as mean ± SD and were analyzed using GraphPad Prism version 8.0 software. The paired *t* test and one-way ANOVA analysis of variance were used for statistical analysis. $p < 0.05$ was considered statistically significant.

Data availability

All data are contained within the article and the supporting information.

Supporting information—This article contains supporting information.

Acknowledgments—We would like to thank Guohui Dang for providing THP-1 cells. This work was supported by the National Natural Science Foundation of China (grant 81571368).

Author contributions—X. Z. and X. L. investigation; X. Z. and X. L. methodology; G. A. project administration; H. J. and J. N. supervision; X. Z. visualization; X. Z. and X. L. writing-original draft; H. J. and J. N. writing-review and editing.

Conflict of interest—The authors declare that they have no conflicts of interest with the contents of this article.

Abbreviations—The abbreviations used are: CYCS, cytochrome c; ICAM1, intercellular cell adhesion molecule 1; LPS, lipopolysaccharide; m^6A, N^6-methyladenosine; METTL3, methyltransferase like 3; NDUFA6, NADH: ubiquinone oxidoreductase subunit A6; NDUFA12, NADH: ubiquinone oxidoreductase subunit A12; NDUFAF1, NADH: ubiquinone oxidoreductase complex assembly factor 1; NDUFB6, NADH: ubiquinone oxidoreductase subunit B6; NDUFC2, NADH: ubiquinone oxidoreductase subunit C2; NDUFV3, NADH: ubiquinone oxidoreductase subunit V3; oxLDL, oxidized low-density lipoprotein; PGC-1α, PPARγ coactivator 1 alpha; PGC-1β, PPARγ coactivator 1 beta; PPARγ, peroxisome proliferator-activated receptor gamma; ROS, reactive oxygen species; TNF-α, tumor necrosis factor-α; UTR, untranslated region; YTHDF1/2/3, YTH N^6-methyladenosine RNA binding protein1/2/3.

References

1. Shi, C., and Pamer, E. G. (2011) Monocyte recruitment during infection and inflammation. *Nat. Rev. Immunol.* **11**, 762–774
2. Auffray, C., Sieweke, M. H., and Geissmann, F. (2009) Blood monocytes: Development, heterogeneity, and relationship with dendritic cells. *Annu. Rev. Immunol.* **27**, 669–692
3. Duffield, J. S. (2010) Macrophages and immunologic inflammation of the kidney. *Semin. Nephrol.* **30**, 234–254

4. Misharin, A. V., Morales-Nebreda, L., Reyfman, P. A., Cuda, C. M., Walter, J. M., McQuattie-Pimentel, A. C., Chen, C.-I., Anekalla, K. R., Joshi, N., Williams, K. J. N., Abdala-Valencia, H., Yacoub, T. J., Chi, M., Chiu, S., Gonzalez-Gonzalez, F. J., *et al.* (2017) Monocyte-derived alveolar macrophages drive lung fibrosis and persist in the lung over the life span. *J. Exp. Med.* **214**, 2387–2404
5. Woollard, K. J., and Geissmann, F. (2010) Monocytes in atherosclerosis: Subsets and functions. *Nat. Rev. Cardiol.* **7**, 77–86
6. Katschke, K. J., Rottman, J. B., Ruth, J. H., Qin, S., Wu, L., LaRosa, G., Ponath, P., Park, C. C., Pope, R. M., and Koch, A. E. (2001) Differential expression of chemokine receptors on peripheral blood, synovial fluid, and synovial tissue monocytes/macrophages in rheumatoid arthritis. *Arthritis Rheum.* **44**, 1022–1032
7. Zuroff, L., Daley, D., Black, K. L., and Koronyo-Hamaoui, M. (2017) Clearance of cerebral Aβ in Alzheimer's disease: Reassessing the role of microglia and monocytes. *Cell Mol. Life Sci.* **74**, 2167–2201
8. Frostegård, J., Nilsson, J., Haegerstrand, A., Hamsten, A., Wigzell, H., and Gidlund, M. (1990) Oxidized low density lipoprotein induces differentiation and adhesion of human monocytes and the monocytic cell line U937. *Proc. Natl. Acad. Sci. U. S. A.* **87**, 904–908
9. Frostegård, J., Wu, R., Giscombe, R., Holm, G., Lefvert, A. K., and Nilsson, J. (1992) Induction of T-cell activation by oxidized low density lipoprotein. *Arterioscler. Thromb.* **12**, 461–467
10. Berliner, J. A., Territo, M. C., Sevanian, A., Ramin, S., Kim, J. A., Bamshad, B., Esterson, M., and Fogelman, A. M. (1990) Minimally modified low density lipoprotein stimulates monocyte endothelial interactions. *J. Clin. Invest.* **85**, 1260–1266
11. Chen, Y., Yang, M., Huang, W., Chen, W., Zhao, Y., Schulte, M. L., Volberding, P., Gerbec, Z., Zimmermann, M. T., Zeighami, A., Demos, W., Zhang, J., Knaack, D. A., Smith, B. C., Cui, W., *et al.* (2019) Mitochondrial metabolic reprogramming by CD36 signaling drives macrophage inflammatory responses. *Circ. Res.* **125**, 1087–1102
12. Zuo, H., and Wan, Y. (2019) Metabolic reprogramming in mitochondria of myeloid cells. *Cells* **9**, 5
13. Villena, J. A. (2015) New insights into PGC-1 coactivators: Redefining their role in the regulation of mitochondrial function and beyond. *FEBS J.* **282**, 647–672
14. Dorn, G. W., and Kitsis, R. N. (2015) The mitochondrial dynamism-mitophagy-cell death interactome: Multiple roles performed by members of a mitochondrial molecular ensemble. *Circ. Res.* **116**, 167–182
15. Finck, B. N., and Kelly, D. P. (2006) PGC-1 coactivators: Inducible regulators of energy metabolism in health and disease. *J. Clin. Invest.* **116**, 615–622
16. Lin, J., Handschin, C., and Spiegelman, B. M. (2005) Metabolic control through the PGC-1 family of transcription coactivators. *Cell Metab.* **1**, 361–370
17. Liu, T. F., Vachharajani, V. T., Yoza, B. K., and McCall, C. E. (2012) NAD+-dependent sirtuin 1 and 6 proteins coordinate a switch from glucose to fatty acid oxidation during the acute inflammatory response. *J. Biol. Chem.* **287**, 25758–25769
18. Dominissini, D., Moshitch-Moshkovitz, S., Schwartz, S., Salmon-Divon, M., Ungar, L., Osenberg, S., Cesarkas, K., Jacob-Hirsch, J., Amariglio, N., Kupiec, M., Sorek, R., and Rechavi, G. (2012) Topology of the human and mouse m6A RNA methylomes revealed by m6A-seq. *Nature* **485**, 201–206
19. Frye, M., Harada, B. T., Behm, M., and He, C. (2018) RNA modifications modulate gene expression during development. *Science* **361**, 1346–1349
20. Vu, L. P., Cheng, Y., and Kharas, M. G. (2019) The biology of mA RNA methylation in normal and malignant hematopoiesis. *Cancer Discov.* **9**, 25–33
21. Zhao, B. S., Roundtree, I. A., and He, C. (2017) Post-transcriptional gene regulation by mRNA modifications. *Nat. Rev. Mol. Cell Biol.* **18**, 31–42
22. Xu, K., Yang, Y., Feng, G.-H., Sun, B.-F., Chen, J.-Q., Li, Y.-F., Chen, Y.-S., Zhang, X.-X., Wang, C.-X., Jiang, L.-Y., Liu, C., Zhang, Z.-Y., Wang, X.-J., Zhou, Q., Yang, Y.-G., *et al.* (2017) Mettl3-mediated mA regulates spermatogonial differentiation and meiosis initiation. *Cell Res.* **27**, 1100–1114
23. Chen, J., Zhang, Y.-C., Huang, C., Shen, H., Sun, B., Cheng, X., Zhang, Y.-J., Yang, Y.-G., Shu, Q., Yang, Y., and Li, X. (2019) mA regulates neurogenesis and neuronal development by modulating histone methyltransferase Ezh2. *Genomics Proteomics Bioinformatics* **17**, 154–168
24. Liu, L., Wang, J., Sun, G., Wu, Q., Ma, J., Zhang, X., Huang, N., Bian, Z., Gu, S., Xu, M., Yin, M., Sun, F., and Pan, Q. (2019) mA mRNA methylation regulates CTNNB1 to promote the proliferation of hepatoblastoma. *Mol. Cancer* **18**, 188
25. Zhang, C., Fu, J., and Zhou, Y. (2019) A review in research progress concerning m6A methylation and immunoregulation. *Front. Immunol.* **10**, 922
26. Zong, X., Zhao, J., Wang, H., Lu, Z., Wang, F., Du, H., and Wang, Y. (2019) Mettl3 deficiency sustains long-chain fatty acid absorption through suppressing Traf6-dependent inflammation response. *J. Immunol.* **202**, 567–578
27. Feng, Z., Li, Q., Meng, R., Yi, B., and Xu, Q. (2018) METTL3 regulates alternative splicing of MyD88 upon the lipopolysaccharide-induced inflammatory response in human dental pulp cells. *J. Cell. Mol. Med.* **22**, 2558–2568
28. Wang, H., Hu, X., Huang, M., Liu, J., Gu, Y., Ma, L., Zhou, Q., and Cao, X. (2019) Mettl3-mediated mRNA mA methylation promotes dendritic cell activation. *Nat. Commun.* **10**, 1898
29. Zhou, Y., Zeng, P., Li, Y.-H., Zhang, Z., and Cui, Q. (2016) SRAMP: Prediction of mammalian N6-methyladenosine (m6A) sites based on sequence-derived features. *Nucleic Acids Res.* **44**, e91
30. Wang, X., Lu, Z., Gomez, A., Hon, G. C., Yue, Y., Han, D., Fu, Y., Parisien, M., Dai, Q., Jia, G., Ren, B., Pan, T., and He, C. (2014) N6-methyladenosine-dependent regulation of messenger RNA stability. *Nature* **505**, 117–120
31. Chimen, M., Evryviadou, A., Box, C. L., Harrison, M. J., Hazeldine, J., Dib, L. H., Kuravi, S. J., Payne, H., Price, J. M. J., Kavanagh, D., Iqbal, A. J., Lax, S., Kalia, N., Brill, A., Thomas, S. G., *et al.* (2020) Appropriation of GPIbα from platelet-derived extracellular vesicles supports monocyte recruitment in systemic inflammation. *Haematologica* **105**, 1248–1261
32. Zhang, Y., Gu, X., Li, D., Cai, L., and Xu, Q. (2019) METTL3 regulates osteoblast differentiation and inflammatory response via Smad signaling and MAPK signaling. *Int. J. Mol. Sci.* **21**, 199
33. Du, H., Zhao, Y., He, J., Zhang, Y., Xi, H., Liu, M., Ma, J., and Wu, L. (2016) YTHDF2 destabilizes m(6)A-containing RNA through direct recruitment of the CCR4-NOT deadenylase complex. *Nat. Commun.* **7**, 12626
34. Wang, X., Huang, N., Yang, M., Wei, D., Tai, H., Han, X., Gong, H., Zhou, J., Qin, J., Wei, X., Chen, H., Fang, T., and Xiao, H. (2017) FTO is required for myogenesis by positively regulating mTOR-PGC-1α pathway-mediated mitochondria biogenesis. *Cell Death Dis.* **8**, e2702
35. Scarpulla, R. C. (2011) Metabolic control of mitochondrial biogenesis through the PGC-1 family regulatory network. *Biochim. Biophys. Acta* **1813**, 1269–1278
36. Evans, M. J., and Scarpulla, R. C. (1989) Interaction of nuclear factors with multiple sites in the somatic cytochrome c promoter. Characterization of upstream NRF-1, ATF, and intron Sp1 recognition sequences. *J. Biol. Chem.* **264**, 14361–14368
37. Li, X., Yang, H., Sun, H., Lu, R., Zhang, C., Gao, N., Meng, Q., Wu, S., Wang, S., Aschner, M., Wu, J., Tang, B., Gu, A., Kay, S. A., and Chen, R. (2017) Taurine ameliorates particulate matter-induced emphysema by switching on mitochondrial NADH dehydrogenase genes. *Proc. Natl. Acad. Sci. U. S. A.* **114**, E9655–E9664
38. Puigserver, P., Wu, Z., Park, C. W., Graves, R., Wright, M., and Spiegelman, B. M. (1998) A cold-inducible coactivator of nuclear receptors linked to adaptive thermogenesis. *Cell* **92**, 829–839
39. Soyal, S., Krempler, F., Oberkofler, H., and Patsch, W. (2006) PGC-1alpha: A potent transcriptional cofactor involved in the pathogenesis of type 2 diabetes. *Diabetologia* **49**, 1477–1488
40. Arena, G., Cissé, M. Y., Pyrdziak, S., Chatre, L., Riscal, R., Fuentes, M., Arnold, J. J., Kastner, M., Gayte, L., Bertrand-Gaday, C., Nay, K., Angebault-Prouteau, C., Murray, K., Chabi, B., Koechlin-Ramonatxo, C., *et al.* (2018) Mitochondrial MDM2 regulates respiratory complex I activity independently of p53. *Mol. Cell* **69**, 594–609.e8
41. Hnasko, T. S., and Hnasko, R. M. (2015) The Western blot. *Methods Mol. Biol.* **1318**, 87–96